Quantifying the terrestrial carbon feedback to anthropogenic carbon emission

Philip Goodwin[1]

6th December 2019

Re-submitted to Earth's Future

[1]Ocean and Earth Science, National Oceanography Centre Southampton, University of Southampton, Southampton, UK

ORCID ID P. Goodwin: 0000-0002-2575-8948

Abstract

The surface warming response to carbon emission is dependent on feedbacks operating in both the physical climate and carbon cycle systems, with physical climate feedbacks quantified via linearly combinable climate feedback terms, $\lambda_{climate}$ in $Wm^{-2}K^{-1}$. However, land carbon feedbacks are often quantified using a two-parameter description, with separate cumulative carbon uptake responses to surface warming, γ_L in PgC K^{-1}, and rising atmospheric CO_2 concentration, β_L in PgC ppm^{-1}. Converting the γ_L and β_L responses to an overall terrestrial carbon feedback parameter, λ_{carbon} in $Wm^{-2}K^{-1}$, has remained problematic, with λ_{carbon} affected by significant non-linear interactions between carbon-climate and carbon-concentration responses and a non-linear relation between atmospheric CO_2 and subsequent radiative forcing. This study presents new relationships quantifying how the overall steady state terrestrial carbon feedback to anthropogenic emission, λ_{carbon}, is dependent on the terrestrial carbon responses to rising CO_2 and temperature, β_L, and γ_L, and the physical climate feedback, $\lambda_{climate}$. Non-linear interactions between β_L and γ_L responses to carbon emission are quantified via a three-parameter description of the land carbon sensitivities to rising CO_2 and temperature. Numerical vegetation model output supports the new relationships, revealing an emerging sensitivity of land carbon feedback to climate feedback of $\partial\lambda_{carbon}/\partial\lambda_{climate}$~0.3. The results highlight that terrestrial carbon feedback and physical climate feedback cannot be considered in

isolation: additional surface warming from stronger climate feedback is automatically compounded by reduced cooling from terrestrial carbon feedback, meanwhile around half the uncertainty in terrestrial carbon feedback originates from uncertainty in the physical climate feedback.

Plain language summary

The amount of surface warming caused by carbon emission is influenced by feedback processes operating in both the physical climate system and in the carbon cycle. Physical climate feedbacks include the responses of clouds, snow and ice cover, atmospheric water vapor and atmospheric lapse rate properties to surface warming. Each of these physical climate feedbacks affects how much warming is generated from a rise in atmospheric carbon dioxide. In contrast carbon cycle feedbacks work in a very different way: by affecting how much of the emitted carbon dioxide is taken up by the land and ocean systems, carbon cycle feedbacks affect how much atmospheric carbon dioxide rises in response to human carbon emission. Since they work in different ways, it has been difficult to directly compare the strengths of physical climate feedbacks with carbon cycle feedbacks. This study identifies a new way of quantifying steady state land carbon cycle feedbacks so that they are easily compared to physical climate feedbacks. A link is also found identifying how land carbon feedbacks remove less carbon dioxide from the atmosphere if physical climate feedbacks cause more warming. In this way, the land carbon feedback could increase additional warming from strong physical climate feedbacks.

1. Introduction

The surface warming response to anthropogenic carbon emission is dependent on feedbacks operating both in the physical climate system (e.g. Knutti et al., 2017) and in the biogeochemical cycling of carbon (e.g. Friedlingstein et al., 2006). Feedbacks operating in the physical climate system include the Planck, water vapor-lapse rate, cloud, and snow and sea-ice albedo feedbacks (e.g. IPCC, 2013). These individual feedbacks are quantified in terms of their climate feedback responses, λ in $Wm^{-2}\ K^{-1}$, which are added together to find the total physical climate feedback, $\lambda_{climate}$ in $Wm^{-2}K^{-1}$ (IPCC, 2013; Knutti et al., 2017)

The land carbon system responds to rising global temperatures and CO_2 levels via a number of feedback mechanisms (e.g. Friedlingstein et al., 2006; IPCC, 2013). The Net Primary Productivity (NPP) of land ecosystems, removing CO_2 from the atmosphere into the land system, is thought to increase with rising atmospheric CO_2 levels through CO_2 fertilisation (e.g. Alexandrov et al., 2003). NPP is also sensitive to global mean temperatures, including via NPP sensitivity to other factors that are themselves linked to changes in global temperature such as the hydrological cycle. The rate of microbial respiration of soil carbon, returning land carbon to the atmosphere, is thought to increase with global mean temperature due to increased metabolic rate (e.g. Friedlingstein et al., 2006). The strengths of all these sensitivities are highly uncertain globally (e.g. IPCC, 2013; Friedlingstein et al.,

2006; Gregory et al., 2009; Arora et al., 2013), in part due to uncertainty in how other factors affect the land carbon system such as nutrient availability. Other land carbon feedback processes occur over long timescales, such as how permafrost thawing releases locked carbon to the atmosphere (e.g. Schuur et al 2015; MacDougall and Knutti, 2016).

Carbon cycle feedbacks, excluding long timescale responses such as permafrost, are often quantified in terms of two sensitivity terms representing the land and ocean carbon cycle responses to rising atmospheric CO_2 and temperature (e.g. Friedlingstein et al., 2006; Gregory et al., 2009; Arora et al., 2013). For the land carbon cycle, the carbon-climate feedback expresses the sensitivity of cumulative land carbon uptake to rising global mean surface temperature, γ_L in PgC K^{-1}, while the carbon-concentration feedback expresses the sensitivity of cumulative land carbon uptake to rising atmospheric CO_2, β_L in PgC ppm^{-1} (e.g. Friedlingstein et al., 2006; Gregory et al., 2009; Arora et al., 2013).

There are difficulties in expressing the overall terrestrial carbon feedback to rising CO_2 and temperature as a λ_{carbon} term in $Wm^{-2}K^{-1}$, such that terrestrial carbon feedbacks can be easily compared to and combined with physical climate feedbacks (e.g. Arora et al., 2013; Gregory et al., 2009). Firstly, the carbon-climate and carbon-concentration feedbacks are interdependent, such that non-linear interactions altering the effective values of γ_L and β_L significantly affect the terrestrial carbon response to a scenario with both rising CO_2 and temperature (Arora et al., 2013; Gregory et al., 2009). Secondly, γ_L and β_L are known to be time-evolving and path dependent, such that their values at any given time depend on history of the temperature and CO_2 (Arora et al., 2013). Thirdly, the land carbon-concentration and carbon-climate feedback terms, γ_L and β_L, calculate the cumulative carbon uptake by the land system in PgC, and not the radiative forcing from the change in atmospheric CO_2 due to land carbon uptake in Wm^{-2}. Gregory et al. (2009) convert γ_L and β_L into a land carbon feedback in $Wm^{-2}K^{-1}$ by:
(1) assuming that the carbon uptake by the land system causes an equal and opposite carbon loss by the atmosphere, and
(2) assuming this carbon loss by the atmosphere (changing atmospheric CO_2 in ppm) relates linearly to the carbon feedback impact on radiative forcing in Wm^{-2}.

However, neither of these assumptions holds when isolating the land carbon feedback. Firstly, although the carbon taken up by the land system does initially originate from the atmosphere, as atmospheric CO_2 is being removed by the land system this inevitably leads to outgassing of CO_2 from the ocean to the atmosphere across the air-sea interface through chemical exchange (e.g. Zeebe and Wolf-Gladrow, 2001). Therefore, the net reduction in atmospheric carbon due to land carbon uptake is

less than the amount of carbon taken up by the land because, due to the induced air-sea exchange, the carbon removed into the land originates from both the atmosphere and ocean (e.g. Goodwin et al., 2008). Note that this effect does not impact the total land and ocean carbon feedback as analysed by Gregory et al. (2009), but only the extraction of the land component. Secondly, radiative forcing in Wm^{-2} is related approximately logarithmically to the change in atmospheric CO_2 (Myhre et al., 2013), such that the same reduction in atmospheric carbon (in PgC or ppm) has approximately half the radiative forcing impact (in Wm^{-2}) if background atmospheric CO_2 is doubled.

Goodwin et al. (2019) recently identified how the magnitudes of terrestrial carbon uptake and surface warming since the preindustrial can be used to calculate the overall land carbon feedback, λ_{carbon} in $Wm^{-2}K^{-1}$, finding $\lambda_{carbon} = 0.31 \pm 0.09$ $Wm^{-2}K^{-1}$ for the present day based on observational reconstructions. However, it is not known how this single land carbon feedback term, λ_{carbon}, relates to the more established land carbon-climate, γ_L, and land carbon-concentration β_L, parameters that are typically evaluated in coupled model simulations (e.g. Friedlingstein et al., 2006; Gregory et al., 2009; Arora et al., 2013).

This study identifies how the steady state terrestrial carbon feedback (λ_{carbon} in $Wm^{-2}K^{-1}$) following anthropogenic carbon emission is related to the land carbon-climate, land carbon-concentration, and physical climate feedbacks (γ_L, β_L and $\lambda_{climate}$ respectively). The relationships account for both the subsequent air-sea exchange of CO_2 due to land carbon uptake, and the logarithmic relationship between atmospheric CO_2 and radiative forcing. The link between λ_{carbon} and $\lambda_{climate}$ is first explored for small perturbations, and then the impact of non-linear interactions between carbon-climate and carbon-concentration responses are quantified, identifying a relationship for λ_{carbon} for large carbon emission perturbations. Using these new relationships for λ_{carbon} this study then shows how the amplification of anthropogenic warming due to terrestrial carbon feedback is dependent on both the Equilibrium Climate Sensitivity (ECS, in K) and carbon emission size, with more likelihood of warming amplification by the terrestrial carbon system when ECS and emission size are large. Note that this steady state analysis does not consider slow land carbon responses with centennial and millennial timescales, such as the permafrost carbon feedback (e.g. Schuur et al 2015; MacDougall and Knutti, 2016).

2 Warming response in the absence of terrestrial carbon feedback

A pulse of CO_2 initially emitted into the atmosphere will eventually partition between the atmosphere, ocean and land systems. The total carbon emitted, $\delta I_{em}(t)$ in PgC, will at any time *t* be equal to the sum of the increases in carbon inventories within the atmosphere, $\delta I_{atm}(t)$, ocean, $\delta I_{ocean}(t)$, and land, $\delta I_{land}(t)$, carbon systems,

$$\delta I_{em}(t) = \delta I_{atm}(t) + \delta I_{ocean}(t) + \delta I_{land}(t) \quad (1)$$

The question is, how will the partitioning of the carbon emission between the atmosphere, ocean and land systems evolve over time? First, consider an atmosphere-ocean only system at an initial steady state, with no carbon exchanges allowed with the land system such that $\delta I_{land} = 0$ in (1) over all time *t*. The atmosphere-ocean system is then perturbed by an instantaneous pulse of carbon emission at time t_0, δI_{em}. At the initial moment of the emission pulse all of the emitted carbon enters the atmosphere, and the increase in atmospheric carbon is therefore equal to the emission pulse size, $\delta I_{em}(t_0) = \delta I_{atm}(t_0)$. Subsequently this rise in atmospheric CO_2 inevitably leads to a flux of carbon into the ocean due to chemical exchange across the air-sea interface and the emitted carbon is now partitioned between the atmosphere and ocean, $I_{em}(t) = \delta I_{atm}(t) + \delta I_{ocean}(t)$.

Over many centuries, the system reaches a new steady state with the carbon emission partitioned between the atmosphere and ocean (Goodwin et al., 2007). Once CO_2 crosses the air-sea interface, it combines with water and dissociates forming three chemical species (e.g. Zeebe and Wolf-Gladrow, 2001) comprising Dissolved Inorganic Carbon (DIC): an uncharged form consisting of aqueous CO_2 and carbonic acid (CO_2^*), a single-charged bicarbonate ion form (HCO_3^-) and a double-charged carbonate ion form (CO_3^{2-}). Air-sea exchange of CO_2 is determined by the CO_2^* component of DIC and, at the preindustrial chemical state, the approximate ratios of CO_2^*:HCO_3^-:CO_3^{2-} are around 1:100:10. However, as more CO_2 dissolves in the ocean seawater becomes more acidic and the relative fraction of DIC composed of CO_2^* increases while the relative fraction composed of CO_3^{2-} decreases.

Due to this non-linear response ocean carbonate chemistry, the fraction of the emitted carbon that remains in the atmosphere depends on the emission size: as more carbon is emitted the ocean becomes more acidic and less soluble to further CO_2. With no land carbon response, the change in atmospheric CO_2 over multi-century timescales, $t=t_{cent}$, once the emitted carbon becomes chemically partitioned between the atmosphere and ocean, is related to the cumulative carbon added to the air-sea system through carbon emission, δI_{em} in PgC, via (Goodwin et al., 2007; 2008; 2009),

$$\delta \ln I_{atm} = \delta \ln \mathrm{CO_2} = \delta I_{em} / I_B \quad (2)$$

using the notation $\delta \ln x = \ln(x + \delta x) - \ln x$, and where I_B is the preindustrial atmosphere-ocean buffered carbon inventory of around 3451±96 PgC in the Climate Model Intercomparison Project phase 5 (CMIP5) models evaluated in Williams et al. (2017). The buffered carbon inventory I_B represents the amount of CO_2 and DIC that is capable of re-distributing between the atmosphere and ocean in the atmospheric CO_2, ocean CO_2^* and ocean CO_3^{2-} pools, and excludes the ocean DIC stored

in the HCO_3^- pool: $I_B \approx I_{atm} + V([CO_2^*] + [CO_3^{2-}])$, where V is the volume of the ocean (*Goodwin et al.*, 2009). Equation (2) holds for carbon emissions up to $\delta I_{em} \sim 5000$ PgC, because the value of I_B can be assumed constant since the increases in I_{atmos} and $V[CO_2^*]$ as more carbon is emitted into the system are opposed by a decrease in $V[CO_3^{2-}]$ (Goodwin et al., 2007; 2009). The impacts of the $CaCO_3$ system on atmospheric CO_2 acting over multimillennial timescales (e.g. Archer, 2005; Goodwin and Ridgwell, 2010) are ignored in this study, which focusses on a century timescale response.

The logarithmic term in equation (2) expresses the impact of non-linear ocean carbonate chemistry on the air-sea partitioning of carbon emitted into the air-sea system: the fraction of emitted carbon remaining in the atmosphere increases with the cumulative carbon emission size, while the fraction of emitted carbon taken up by the ocean decreases with emission size, due to the decreasing solubility of CO_2 in seawater as the ocean becomes more acidic (see also e.g. Zeebe and Wolf-Gladrow, 2001). Thus, the nature of ocean carbonate chemistry implies that a constant sensitivity of ocean carbon uptake, δI_{ocean}, to atmospheric CO_2, via either δCO_2 or δI_{atm}, cannot be defined: the sensitivity is itself dependent on the atmospheric CO_2 level. Therefore, this study refrains from attempting to define an ocean carbon-concentration feedback strength (e.g. see Friedlingstein et al., 2006), β_{ocean}, in units of PgC ocean uptake per unit ppm increase in atmospheric CO_2. Instead, ocean carbonate chemistry is utilised to express the sensitivity of ocean carbon uptake to atmospheric CO_2 via (2). Note that the non-linear ocean carbonate chemistry does not affect the ability to define a land carbon-concentration feedback, β_L.

The rise in CO_2 from carbon emission in (2) induces a radiative forcing (Myhre et al., 2013) which in turn induces a surface warming (Williams et al., 2012). The radiative forcing from the increase in CO_2 due to carbon emission, δR_{CO2}^{em}, is related to the increase in the log of atmospheric CO_2, $\delta R_{CO2}^{em} = a\delta \ln CO_2$, where a=5.35±0.27 Wm^{-2} is the CO_2 radiative forcing coefficient (Myhre et al., 2013), making δR_{CO2}^{em} linearly related to carbon emission (2) (Goodwin et al., 2009). This radiative forcing from carbon emission induces surface warming until the radiative forcing is balanced by an increase in outgoing radiation from elevated surface temperatures, $\lambda_{climate}\delta T_0$ in Wm^{-2}, via,

$$\lambda_{climate}\delta T_0 = \delta R_{CO2}^{em} = a\delta \ln CO_2 = \frac{a}{I_B}\delta I_{em} \quad (3)$$

where δT_0 is the steady state temperature change from carbon emission in the absence of terrestrial carbon response in K, and $\lambda_{climate}$ is the climate feedback in $Wm^{-2}K^{-1}$. The climate feedback is formally defined as the sensitivity of Earth's net radiation balance to changes in surface temperature, $\lambda_{climate} = -\delta R^{feedback}/\delta T$, where $\delta R^{feedback}$ is the change in net downward energy flux at the

top of the atmosphere due to the change in global mean surface temperature, δT. Note that the sign convention adopted here is such that $\lambda_{climate}$ is positive, because a surface warming ($\delta T > 0$) causes a net *upward* radiation flux ($R^{feedback} < 0$). The next section considers how this relationship between warming and emissions (3) is altered by the presence of a terrestrial carbon system for small perturbations.

3. Impact of terrestrial carbon feedback for small perturbation

Section 3.1 finds a relationship to calculate steady state λ_{carbon} following a small carbon emission, in terms of $\lambda_{climate}$, β_L and γ_L. Section 3.2 tests this relationship using numerical model simulations.

3.1 Theory

Now consider an atmosphere-ocean-land system at an initial steady state then perturbed by a CO_2 emission, with no perturbations to other sources of radiative forcing. Once the system reaches a new steady state, the carbon emission will be partitioned between the atmosphere, ocean and land systems. The component of emitted carbon that remains in the atmosphere will increase atmospheric CO_2 and induce a radiative forcing that causes a rise in surface temperatures.

Terrestrial carbon storage, I_{ter} in PgC, is sensitive to changes in both atmospheric CO_2 levels and climate, with global mean surface temperature commonly used to represent the level of climate change (e.g. *Friedlingstein et al*., 2006). At steady state, a small perturbation in terrestrial carbon storage, δI_{ter} in PgC, is related to small perturbations in atmospheric CO_2, $\delta \mathrm{CO}_2$ in ppm, and global mean surface temperature change, δT in K, via,

$$\delta I_{ter} = \left.\frac{\partial I_{ter}}{\partial \mathrm{CO}_2}\right|_T \delta \mathrm{CO}_2 + \left.\frac{\partial I_{ter}}{\partial T}\right|_{\mathrm{CO2}} \delta T = \beta_L \delta \mathrm{CO}_2 + \gamma_L \delta T \tag{4}$$

The empirically determined carbon-concentration feedback, $\beta_L = \left.\frac{\partial I_{ter}}{\partial \mathrm{CO}_2}\right|_T$ in PgC ppm^{-1}, and carbon-climate feedback, $\gamma_L = \left.\frac{\partial I_{ter}}{\partial T}\right|_{\mathrm{CO2}}$ in PgC K^{-1}, represent the cumulative terrestrial carbon uptake sensitivities to atmospheric CO_2 (at constant preindustrial temperature) and global mean surface warming (at constant preindustrial CO_2) respectively, following the framework set out in *Friedlingstein et al*. (2006). Note that β_L may change with background temperature and γ_L may change with background CO_2, leading to significant non-linearities between the carbon-climate and carbon-concentration feedbacks (Gregory et al., 2009; Arora et al., 2013). Therefore, (4) is only strictly applicable to small perturbations.

Relative to the case in the absence of terrestrial carbon feedback (eqns. 2, 3), this change in terrestrial carbon storage (4) will alter the steady state rise in atmospheric CO_2 (1), and so also alter the radiative forcing from atmospheric CO_2 and the global mean surface warming (3). For a hypothetical atmosphere-land only system, with no coupled ocean, an increase in land carbon storage would cause and equal and opposite decrease in atmospheric carbon storage. However, for a coupled atmosphere-ocean-land carbon system, an increase in land carbon storage leads to, and is balanced by the sum of, decreases in both the atmosphere and ocean carbon storage. Initially, the additional carbon stored in the land system comes from the atmosphere, but over time this decrease in atmospheric CO_2 then causes an inevitable ocean outgassing due to air-sea chemical exchange. By similarity to equation (2), we find that the change in atmospheric CO_2 over multi-century timescales due to an initial uptake of carbon by the terrestrial system, after accounting for subsequent air-sea gas exchange, is given by (Goodwin et al., 2008),

$$\delta \ln I_{atmos} = \delta \ln \mathrm{CO}_2 = -\delta I_{ter}/I_B \tag{5}$$

where the carbon added to the air-sea system in (2) due to emission, δI_{em}, is replaced here by the carbon added to the air-sea system by terrestrial carbon uptake, $-\delta I_{ter}$, noting the minus sign arises because an increase in terrestrial carbon storage removes carbon from the air-sea system.

When terrestrial carbon uptake is considered in the context of a coupled atmosphere-ocean-land carbon system peterbed by anthropogenic carbon emission, the atmosphere-ocean relationship for the total log CO_2 change at steady state, eq. (2), is modified to contain an additional term representing how the total carbon added to the air-sea system now has contributions from both carbon emission, δI_{em}, and terrestrial carbon uptake, $-\delta I_{ter}$, (Goodwin et al., 2007; 2008; 2009; 2015), giving,

$$\delta \ln I_{atmos} = \delta \ln \mathrm{CO}_2 = \frac{\delta I_{em}}{I_B} - \frac{\delta I_{ter}}{I_B} \tag{6}$$

This relationship calculates the long-term atmospheric CO_2 change in response to carbon emission and terrestrial carbon uptake, accounting for the inevitable air-sea gas exchange over many centuries through the I_B terms.

Considering (5) and (6), the total radiative forcing from CO_2, $\delta R_{CO2} = a\delta \ln \mathrm{CO}_2$, now has components from carbon emission, $\delta R_{CO2}^{em} = (a/I_B)\delta I_{em}$: eq. (3), and from terrestrial carbon response to rising CO_2 and temperature, $\delta R_{CO2}^{ter} = -(a/I_B)\delta I_{ter}$, via (*Goodwin et al.*, 2008; 2009; 2015)

$$\delta R_{CO2} = \delta R_{CO2}^{em} + \delta R_{CO2}^{ter} = \frac{a}{I_B}\delta I_{em} - \frac{a}{I_B}\delta I_{ter} \tag{7}$$

where δR_{CO2}^{ter} represents radiative forcing from the terrestrial carbon feedback accounting for both terrestrial carbon uptake and the subsequent air-sea gas exchange.

The rise in surface temperature from carbon emission in the presence of terrestrial carbon uptake, δT in K, is then given by this total radiative forcing accounting for both the emissions and terrestrial carbon response, noting the identity $\delta \ln x = \delta x/x$,

$$\lambda_{climate}\delta T = \delta R_{CO2} = a\delta \ln \mathrm{CO_2} = \frac{a}{\mathrm{CO_2}}\delta \mathrm{CO_2} \tag{8}$$

The climate feedback may be considered in terms of the change in Earth's radiation balance from physical climate system induced changes per unit increase in surface temperature: $\lambda_{climate} = -\delta R^{feedback}/\delta T$. By similarity, we may define the terrestrial carbon feedback in terms of the change in Earth's energy balance from terrestrial carbon system induced changes in atmospheric CO_2 per unit surface warming (Goodwin et al., 2019): $\lambda_{carbon} = -\delta R_{CO2}^{ter}/\delta T$ in $\mathrm{Wm^{-2}K^{-1}}$.

Substituting $\delta \mathrm{CO_2} = (\lambda_{climate}\mathrm{CO_2}/a)\delta T$ from (8) into (4), reveals $\delta I_{ter} = \beta_L(\lambda_{climate}\mathrm{CO_2}/a)\delta T + \gamma_L \delta T$ and then dividing both sides by δT gives $\delta I_{ter}/\delta T = \beta_L(\lambda_{climate}\mathrm{CO_2}/a) + \gamma_L$. Finally, multiplying both sides by a/I_B, to express δI_{ter} in terms of δR_{CO2}^{ter} using (7), $\delta R_{CO2}^{ter} = -(a/I_B)\delta I_{ter}$, reveals how steady state terrestrial carbon feedback, λ_{carbon}, is related to $\lambda_{climate}$, β_L and γ_L,

$$\lambda_{carbon} = -\frac{\delta R_{CO2}^{ter}}{\delta T} = \frac{a}{I_B}\frac{\delta I_{ter}}{\delta T} = \frac{\mathrm{CO_2}}{I_B}\beta_L\lambda_{climate} + \frac{a}{I_B}\gamma_L \tag{9}$$

This relationship (9) solves for the terrestrial carbon feedback following carbon emission once atmosphere-ocean-land carbon partitioning has reached a steady state, and temperatures have stabilized with respect to the elevated atmospheric CO_2. Equation (9) predicts that, for given land carbon-concentration and carbon-climate responses to an infinitesimal carbon emission, the carbon feedback, $\lambda_{Carbon} = -\delta R_{CO2}^{ter}/\delta T$, is linearly related to climate feedback, $\lambda_{climate}$. Using the mean and standard deviation values of β_L (0.92±0.44 PgC $\mathrm{ppm^{-1}}$) and γ_L (-58.4±28.5 PgC $\mathrm{K^{-1}}$), from the CMIP5 models evaluated by Arora et al. (2013) following a $4\times\mathrm{CO_2}$ experiment, eq. (9) predicts: $\lambda_{carbon} = (0.30 \pm 0.14)\lambda_{climate} + (-0.09 \pm 0.04)$, assuming normal error propagation and adopting $I_B = 3451 \pm 96$ PgC, $a = 5.35 \pm 0.27$ $\mathrm{Wm^{-2}}$, and CO_2=1120 ppm.

Diagnosing λ_{carbon} from land carbon uptake, δI_{ter}, and surface warming, δT, using eq. (9) rests on two assumptions: the use of the buffered carbon inventory I_B to calculate $\delta \ln CO_2$, and the use of the radiative forcing coefficient, a, to calculate the radiative forcing from $\delta \ln CO_2$. The discrepancy in $\delta \ln CO_2$ as predicted using I_B via eqns. (2) or (6) remains under 3% for carbon perturbation up to the approximate magnitude of the entire land carbon reservoir, $\delta I_{ter} \sim 2000$ PgC, when compared to multi-century numerical simulations with explicit representations of ocean carbonate chemistry (Goodwin et al., 2007). Once partitioned between the atmosphere and ocean, a $\delta I_{ter} \sim 2000$ PgC magnitude perturbation would change atmospheric CO_2 by around $\delta \ln CO_2 \sim 2000/I_B \sim 0.6$. The discrepancy in δR_{CO2} when using $\delta R_{CO2} = a\delta \ln CO_2$, with $a = 5.35$ Wm^{-2}, is around 5% when compared to calculations containing second order terms ($\delta R_{CO2} = 5.32\delta \ln CO_2 + 0.26[\delta \ln CO_2]^2$: Byrne and Goldblatt, 2014). Thus, the two assumptions in equation (9) are valid for plausible magnitude land carbon perturbations.

Utilizing (9) and (7) in (8) then relates steady state surface warming to cumulative carbon emission in the presence of terrestrial carbon responses to rising CO_2 and temperature,

$$(\lambda_{climate} + \lambda_{carbon})\delta T = \delta R_{CO2}^{em} = \frac{a}{I_B}\delta I_{em} \tag{10}$$

Inspecting equation (10) shows that λ_{carbon} is directly comparable to, and linearly combinable with, physical climate feedbacks evaluated in Wm^{-2}K^{-1} such as the water vapor-lapse rate and cloud feedbacks that make up $\lambda_{climate}$ (Knutti et al., 2017; IPCC, 2013).

3.2 Comparison of theory to numerical model output

This section tests the prediction from (9) that λ_{carbon} is linearly related to $\lambda_{climate}$ under a fixed CO_2 perturbation using numerical Dynamic Global Vegetation Model (DGVM) output from Pugh et al. (2018) and output from an efficient Earth system model (Goodwin, 2016; 2018).

3.2.1 Descriptions of model output

Pugh et al. (2018) integrate a single DGVM (the TRIFFID model) to steady state with the same CO_2 perturbation (from preindustrial to ~850 ppm), but with 22 different climatic responses to that CO_2 perturbation (Pugh et al., 2018: the 'climate' ensemble therein). The steady state cumulative carbon uptake for each of the 22 DGVM simulations, ΔI_{ter}, shows a general increasing trend with the effective value of $\lambda_{climate}$ (Fig. 1a, black dots), where $\lambda_{climate}$ is diagnosed here from the model temperature response to CO_2 using a=5.35 Wm^{-2}: $\lambda_{climate} = a\Delta \ln CO_2/\Delta T$.

Separately, an ensemble of 6270 observation-constrained simulations of the efficient Warming Acidification and Sea level Projector (WASP) Earth system model (Appendix A: Goodwin, 2016; 2018; Goodwin et al., 2019) are integrated to steady state following a 1-year increase in CO_2 from 280ppm to 850 ppm. The ensemble of 6270 simulations are generated from the Monte Carlo combined with history matching approach set out in Goodwin et al. (2018), using the WASP model configuration of Goodwin (2018). In this configuration the value of $\lambda_{climate}$ is allowed to vary over multiple response timescales linked to the different timescales of climate feedback processes (Goodwin, 2018). For example, there is an instantaneous contribution to $\lambda_{climate}$ from the Planck feedback, while contributions from the fast cloud response and water vapor-lapse rate response occur over order 10 days linked to the residence time of water vapor in the atmosphere, and contributions to $\lambda_{climate}$ from the way that changes in sea surface warming pattern alter the cloud response occur over decades.

The Monte Carlo combined with history matching method generates 6270 observation-consistent simulations in the following way. First, an initial ensemble of 10 million simulations is generated with varying model parameter values, using the parameter input distributions of Goodwin (2018). The model parameters for climate feedback from different processes are varied to span the ranges evaluated in CMIP5 models (Goodwin, 2018). Also, the initial ensemble sensitivities of terrestrial Net Primary Productivity (NPP) and soil carbon residence time to global temperature and CO_2 are varied to span the range of sensitivities seen the in the C4MIP models analysed by Freidlingstein et al. (2006 – see Fig. 3 therein). These 10 million initial simulations are integrated from preindustrial to present day and evaluated for observational consistency against observational reconstructions of surface warming (IPCC, 2013; Morice et al., 2012; Hansen et al., 2012; Smith et al., 2008; Vose et al., 2012), ocean heat content (Levitus et al., 2012; Giese and Ray, 2011; Balmaseda et al., 2013; Good et al., 2013; Smith et al., 2015; Cheng et al., 2017) and ocean and terrestrial carbon uptake (IPCC, 2013; le Quéré et al., 2018) after Goodwin et al (2018). The observation consistency test of Goodwin (2018 – see Table 2 therein) is applied, adapted here after Goodwin et al. (2019) with an updated cumulative terrestrial carbon uptake constraint based on the Global Carbon Budget analysis (le Quéré et al., 2018) (Appendix A).

A total of 6273 simulations pass the updated observation-consistency test. Three of these simulations are excluded as non-physical, since their values of $\lambda_{climate}$ become negative on long timescales, leaving a final ensemble of 6270 observation-consistent simulations (Goodwin et al., 2019). This final ensemble therefore contains ranges of terrestrial carbon sensitivities to temperature and CO_2 that agree with both the analysed sensitivities of the C4MIP models (Friedlingstein et al., 2006) and observational reconstructions of cumulative carbon uptake (le Quéré et al. 2018).

Each of the 6270 observation-consistent ensemble members are reinitialised to preindustrial conditions, and forced with a 1-year step function increase in CO_2 from 280 ppm to 850 ppm. Each ensemble member is then integrated for 500 years to reach a new steady state, without any imposed noise in the surface temperature. The values of ΔI_{ter} and $\lambda_{climate}$ in the efficient model simulations are diagnosed at the end of the 500-year simulations to represent the new steady state reached. The observation-consistent ensemble of efficient model simulations shows a similar increasing trend in steady state ΔI_{ter} at high $\lambda_{climate}$ (Fig. 1a, blue transparent dots) to the DGVM simulations (Fig. 1a, black dots), but with greater variation reflecting the greater extent of parameter space explored.

3.2.2 Results from model output

Next, for the 22 DGVM and 6270 efficient model simulations, λ_{carbon} is calculated from ΔI_{ter} and ΔT using eq. (9): $\lambda_{carbon} = -\delta R^{ter}_{CO2}/\delta T = (a\delta I_{ter})/(I_B \delta T)$ (Appendix A). The emergent linear link between steady state carbon feedback and climate feedback predicted from theory (eq. 9) is identified on both the DGVM ensemble (Fig. 1b, black) and an efficient model ensemble (Fig. 1, blue). In the DGVM simulations, with identical carbon cycle configurations, over 90% of the variance in λ_{carbon} is explained by the variation in $\lambda_{climate}$ (Fig. 2b, black: R^2=0.96). The efficient model ensemble contain variation in the carbon cycle model parameter values (Goodwin, 2018), and so will have variation in the effective values of β_L and γ_L between ensemble members. Despite this variation, around half of the variance in λ_{carbon} is explained by the variation in $\lambda_{climate}$ (Fig. 2b, blue: R^2=0.49). This demonstrates the robustness of the emergent link identified between terrestrial carbon and physical climate feedback, λ_{carbon} and $\lambda_{climate}$ (eq. 9). The sensitivity of λ_{carbon} to $\lambda_{climate}$ of ~0.3 in the DGVM and efficient model ensembles (Fig. 1b) is consistent with the sensitivity predicted using eq. (9) for the CMIP5 model values of β_L and γ_L. Note that the analysis here is for steady state λ_{carbon}, but that for transient cases λ_{carbon} will vary over time as δI_{ter} and δT vary (Goodwin et al, 2019).

4. Impact of terrestrial carbon feedback for large perturbation

Non-linear terms will affect the terrestrial carbon uptake response for large emission sizes, leading to errors when applying β_L and γ_L using eq. (4) (e.g. Arora et al., 2013; Gregory et al., 2009). The question is, how will carbon feedback, λ_{carbon}, alter for large emission perturbations due to these non-linear terms compared with the expected value for small perturbations, eq. (9)?

Here, instead of representing the sensitivity of the terrestrial carbon cycle to rising CO_2 and temperature via the carbon climate and carbon CO_2 feedback parameters, $\beta_L = \left.\frac{\partial I_{ter}}{\partial \mathrm{CO_2}}\right|_T$ and $\gamma_L = \left.\frac{\partial I_{ter}}{\partial T}\right|_{\mathrm{CO2}}$ respectively, the terrestrial carbon system is characterized in terms of empirical feedback

parameters for aspects of the carbon system that allow non-linear interactions between carbon cycle responses to temperature and CO_2 to be considered.

First, consider a simple two box representation of the terrestrial carbon cycle coupled to an atmosphere (Fig. 2), where the total terrestrial carbon storage, I_{ter}, is the sum of the soil carbon reservoir, I_{soil} in PgC, and the vegetation carbon reservoir, I_{veg} in PgC: $I_{ter} = I_{veg} + I_{soil}$. The vegetation carbon pool has an incoming carbon flux from the atmosphere due to Net Primary Productivity (NPP), F_{NPP} in PgC yr^{-1}. There is then a flux from the vegetation carbon pool into the soil carbon pool due to leaf litter, $F_{leaflitter}$ in PgC yr^{-1}, and a flux from the soil carbon pool into the atmosphere due to soil carbon respiration, $F_{respiration}$ in PgC yr^{-1} (Fig. 2). At steady state the leaf litter and soil carbon respiration carbon fluxes must equal NPP, $F_{NPP} = F_{Leaflitter} = F_{respiration}$, and note that a subscript 0 is used to denote the value of a quantity at the initial steady state (Fig. 2).

Next, consider the carbon fluxes in the terrestrial carbon system to be sensitive to atmospheric CO_2 and temperature via the following parameters (Fig. 2):
(1) A dimensionless CO_2 fertilization coefficient (Alexandrov et al., 2003) representing the fractional change in NPP flux per unit log change in CO_2, β_{CO2}, such that at constant temperature $F_{NPP} = F_{NPP,0}(1 + \beta_{CO2}\delta \ln \mathrm{CO_2})$;
(2) A coefficient representing the fractional change in NPP per unit change in global mean surface temperature, c_{NPP} in K^{-1}, such that at constant CO_2 $F_{NPP} = F_{NPP,0}(1 + c_{NPP}\delta T)$; and
(3) A coefficient representing the fractional change in soil carbon residence time, τ_{soil} in yr, per unit change in global mean surface temperature, c_{soil} in K^{-1}, such that $\tau_{soil} = \tau_{soil,0}(1 + c_{soil}\delta T)$ where $F_{respiration} = I_{soil}/\tau_{soil}$.

Adopting this representation for the CO_2 and T dependences of carbon fluxes within the land carbon system (Fig. 2) allows the steady state terrestrial carbon storage be expressed in terms of the log CO_2 and warming perturbations, $\delta \ln \mathrm{CO_2}$ and δT, the initial NPP, $F_{NPP,0}$, and the initial residence timescales of carbon in the vegetation and soil carbon pools, $\tau_{veg,0}$ and $\tau_{soil,0}$ respectively, via (Appendix B)

$$I_{ter} = F_{NPP,0}(1 + \beta_{CO2}\delta \ln \mathrm{CO_2})(1 + c_{NPP}\delta T)\left(\tau_{veg,0} + \tau_{soil,0}[1 + c_{soil}\delta T]\right) \quad (11)$$

Note that this equation (11) solves for the steady state terrestrial carbon storage, I_{ter}, for defined values of CO_2 and T, and so time-dependencies are not shown. However, if the terrestrial carbon reservoir responds more quickly than slowly evolving changes in temperature or CO_2, then (11) still applies and the terms in I_{ter}, $\delta \ln \mathrm{CO_2}$ and δT can be considered time-dependent.

Substituting steady state relationships for $\delta \ln \mathrm{CO}_2 = (\lambda_{climate}\mathrm{CO}_2/a)\delta T$ and $\lambda_{carbon} = -\delta R^{ter}_{CO2}/\delta T = (a\delta I_{ter})/(I_B \delta T)$, from (8) and (9) respectively, into eq. (11) results in a second-order polynomial equation for λ_{carbon} in δT (Appendix B),

$$\lambda_{carbon} = \left(\lambda_{climate}\frac{I_{ter,0}}{I_B}\beta_{CO2} + a\frac{I_{ter,0}}{I_B}c_{NPP} + a\frac{I_{soil,0}}{I_B}c_{soil}\right) + \left(\lambda_{climate}\frac{I_{ter,0}}{I_B}\beta_{CO2}c_{NPP} + \lambda_{climate}\frac{I_{soil,0}}{I_B}\beta_{CO2}c_{soil} + a\frac{I_{soil,0}}{I_B}c_{NPP}c_{soil}\right)\delta T + \left(\lambda_{climate}\frac{I_{soil,0}}{I_B}\beta_{CO2}c_{NPP}c_{soil}\right)\delta T^2 \quad (12)$$

This relationship for steady state terrestrial carbon feedback, λ_{carbon}, preserves non-linear interactions between carbon-concentration and carbon-temperature responses, eq. (12). It is noted that additional non-linearities affecting λ_{carbon} may exist that are not captured in (12), if the values of the coefficients β_{CO2}, c_{NPP} and c_{soil} change with perturbation size.

By inspecting the leading order terms in (12), and comparing to (9), we can express the carbon-concentration and carbon-climate feedbacks in terms of the alternative carbon-system parameters, β_{CO2}, c_{NPP} and c_{soil}: $\beta_L \approx \frac{I_{ter,0}}{\mathrm{CO}_2}\beta_{CO2}$ and $\gamma_L \approx I_{ter,0}c_{NPP} + I_{soil,0}c_{soil}$.

In eq. (12) the term in δT is much larger than the term in δT^2 for reasonable temperature changes and parameter values. Therefore, the sensitivity of λ_{carbon} to surface warming, at constant $\lambda_{climate}$, from the non-linear interactions between terrestrial carbon-climate and carbon-concentration responses simplifies to,

$$\left.\frac{\partial \lambda_{carbon}}{\partial T}\right|_{\lambda_{climate}} \approx \lambda_{climate}\frac{I_{ter,0}}{I_B}\beta_{CO2}c_{NPP} + \lambda_{climate}\frac{I_{soil,0}}{I_B}\beta_{CO2}c_{soil} + a\frac{I_{soil,0}}{I_B}c_{NPP}c_{soil} \quad (13)$$

Noting that c_{soil} and c_{NPP} are likely negative (see Friedlingstein et al., 2006 - figure 3 therein), eq. (13) therefore predicts that there will be a near-linear decrease in λ_{Carbon} as the perturbation in δT is increased for a given value of $\lambda_{climate}$. Example carbon sensitivity values suggests a linear reduction in λ_{carbon} with increasing temperature anomaly of order $\partial\lambda_{carbon}/\partial T \sim -0.015$ $\mathrm{Wm^{-2}K^{-2}}$: using β_{CO2}~0.45, $c_{NPP}\sim -0.04$ $\mathrm{K^{-1}}$ and $c_{soil}\sim -0.02$ $\mathrm{K^{-1}}$ (each within the range of the Earth system models analyzed in Friedlingstein et al., 2006 – figure 3 therein), along with $\lambda_{climate} = 1.2$ $\mathrm{Wm^{-2}K^{-1}}$, a =5.35 $\mathrm{Wm^{-2}}$ (Myhre et al., 2013), I_B=3451 PgC (Williams et al., 2017), $I_{ter,0}$=2000PgC, and $I_{soil,0}$=1500PgC. Note that a positive λ_{carbon} implies that terrestrial carbon feedback is negative,

reducing surface warming, and so from (13) terrestrial carbon feedback is expected to become a less negative feedback (or even a positive feedback) with increasing temperature anomaly.

4.2 Comparison of theory to numerical model output

This section tests the prediction from (13), that λ_{carbon} linearly reduces with perturbation size δT for a given value of $\lambda_{climate}$, using published numerical DGVM output (Pugh et al., 2018) and output from the observation-consistent ensemble of 6270 efficient Earth system model (Goodwin et al., 2016; 2018) simulations (Fig. 3).

4.2.1 Descriptions of model output

Pugh et al. (2018) integrate multiple DVGMs to steady state under CO_2 forced climate scenarios with warming of ΔT = 1, 2, 3, 4, and 5 K (Pugh et al., 2018 – 'DGVM ensemble' therein, using HYLAND, SDGVM, ORCHIDEE, TRIFFID, LPJ models), and also integrate a DGVM within a coupled Earth system model at multiple CO_2 forcing scenarios achieving different levels of warming (the HadCM3LC simulations in Pugh et al., 2018). In these DVGM simulations (Pugh et al., 2018), the magnitude of steady state cumulative land carbon uptake, ΔI_{ter}, initially increases with ΔT for CO_2 only forcing (Fig. 3a, dots, diamonds and dashed lines). However, the rate of increase in ΔI_{ter} per unit additional surface warming reduces for all DVGMs, with some models showing a rate of decrease per unit additional warming as total warming nears 5K (Fig. 3a).

The 6270 efficient WASP model simulations are re-initialized to a preindustrial steady state and perturbed this time with carbon emissions scenarios that interactively restores atmospheric CO_2 to produce a range of specified surface warming targets, of ΔT = 1, 2, 3, 4, and 5 K (for description of the restoring method used in the WASP model see Nichols et al., 2018). Again, the simulations are integrated without imposed noise in the surface temperature (Goodwin, 2018). For each warming target, all 6270 simulations are integrated for 500 years until a new steady state is reached. Global mean surface temperature anomaly is stabilized to within ±0.02 K of the desired target in at least 99% of the 6270 simulations. This efficient model ensemble shows a similar pattern of change in steady state ΔI_{ter} with increasing steady state ΔT to the DVGMs (Fig 3a, compare blue solid line and shading to black and color dots, grey diamonds and associated dashed lines):

4.2.2 Results from model output

Terrestrial carbon feedback, λ_{carbon}, is diagnosed from the model output (Fig. 3a) using $\lambda_{carbon} = -\delta R_{CO2}^{ter}/\delta T = (a\delta I_{ter})/(I_B \delta T)$, where a=5.35 Wm^{-2} (Myhre et al., 2013) and I_B=3451 PgC (Williams et al., 2017) is assumed for the DGVMs (Fig. 3b, dots, diamonds and dashed lines) and a and I_B are individually assessed for each WASP ensemble member (Fig. 3b, blue solid line and

shading). This reveals a near-linear decrease in λ_{carbon} with ΔT for both DGVM simulations and the efficient model ensemble (Fig. 3b), in agreement with the prediction made from eq. (13). The sensitivity of terrestrial carbon feedback to surface temperature lies in the range $\partial\lambda_{carbon}/\partial T$ ~-0.01 to -0.07 $Wm^{-2}K^{-2}$ for the DGVMs and most of the efficient model ensemble (Fig. 3c), with a small number of efficient model simulations showing a small positive sensitivity (Fig. 3c, blue solid line and shading).

The reduction in λ_{carbon} for larger perturbations in δT in the DGVM and efficient model simulations (Fig. 3) shows that the non-linear interactions between carbon-climate and carbon-concentration feedbacks (eq. 9) are significant for large carbon emissions, in agreement with previous studies (e.g. Arora et al., 2013; Gregory et al., 2009), implying that the standard β_L and γ_L representation of the terrestrial carbon feedback may lead to significant error.

The agreement between the predicted near-linear decrease in λ_{carbon} with increasing δT from eqns. (12, 13) and the behaviour of the ensemble of DGVM simulations (Fig. 3), indicates that non-linearities between terrestrial carbon-climate and carbon-concentration feedbacks may be captured by considering a relatively simple representation of the terrestrial carbon cycle (Fig. 2; Appendix B). This simple representation includes three empirically determined sensitivities: a dimensionless CO_2 fertilisation sensitivity of NPP, β_{CO2}; a temperature sensitivity of NPP, c_{NPP} in K^{-1}; and a temperature sensitivity of the soil carbon respiration timescale, c_{soil} in K^{-1} (Appendix equations B4, B5). Note that additional non-linearities may become significant for the real terrestrial carbon cycle that are not captured in the DGVM simulations.

5. Implications for gain in surface warming from terrestrial carbon feedback

A gain factor for land carbon feedback on surface warming, G_L, may be defined as the ratio of warming in presence of terrestrial carbon feedback divided by warming in the absence of terrestrial carbon feedback (Gregory et al., 2009). G_L is expressed in terms of either the emission size and change in terrestrial carbon reservoir, or the carbon and climate feedbacks, as,

$$G_L = \frac{\delta T}{\delta T_0} = \frac{\delta I_{em}}{\delta I_{em} - \delta I_{ter}} = \frac{\lambda_{climate}}{\lambda_{climate} + \lambda_{carbon}} \quad (14a)$$

where eqns. (9) and (12) show how λ_{carbon} relates to $\lambda_{climate}$ for infinitesimal and finite carbon emission perturbations respectively. For infinitesimal emission perturbations, where non-linear interactions between CO_2 and T responses of terrestrial carbon cycle can be ignored, the gain G_L becomes,

$$G_L = \left(1 + \frac{\mathrm{CO_2}}{I_B}\beta_L + \frac{a}{\lambda_{climate} I_B}\gamma_L\right)^{-1} = \left(1 + \frac{\mathrm{CO_2}}{I_B}\beta_L + \frac{\mathrm{ECS}}{I_B \ln 2}\gamma_L\right)^{-1}$$

(14b)

β_L is likely positive, since Net Primary Productivity (NPP) increases with rising CO_2 due to CO_2 fertilization. However, γ_L is negative in many models (Arora et al., 2013), since soil carbon storage decreases with rising T as soil carbon residence time reduces (Friedlingstein et al., 2006). This means that the gain factor for terrestrial carbon feedback, G_L, will increase at higher ECS or lower $\lambda_{climate}$ (14) (Fig. 1b).

By inspecting how λ_{carbon} changes for different values of $\lambda_{climate}$ for the DGVM and efficient model ensemble output in Figure 1b, and converting $\lambda_{climate}$ into ECS, we can see from eq. (14a) that the gain G_L<1 for ECS ≤ 5.8K (Fig. 4, solid black and blue lines), such that terrestrial carbon feedback reduces surface warming from anthropogenic carbon emissions. However, the gain switches to G_L>1 (eq. 14a) for ECS ≥ 5.9 K, such that the terrestrial carbon feedback increases surface warming from carbon emissions (Fig. 4). For larger perturbation sizes (Fig 3, eq. 13), the non-linear interactions cause the carbon feedback to become less negative (or more positive), and so the ECS value above which terrestrial feedbacks switch from damping to amplifying anthropogenic warming would decrease. Other model ensembles may yield different results. The values of β_L and γ_L from the CMIP5 models analysed by Arora et al. (2013), when applied to equation (14b) and considering perturbations that stabilize CO_2 at approximately present-day levels (CO_2=410 ppm), suggest considerable uncertainty in the value of ECS above which gain transitions from damping gain, $G_L < 1$, to amplifying gain, $G_L > 1$ (Fig. 4, solid orange line and colour dashed lines). The CMIP5 multi-model mean values of β_L and γ_L (Arora et al., 2013) suggest land carbon feedbacks amplify steady state warming for ECS above 4.5 K (G_L>1) and dampen steady state warming below ECS of 4.5 K (G_L<1), for CO_2 stabilisation at 410ppm (Fig. 4, solid orange line). However, the ECS values above which land carbon feedback amplifies steady state warming range from a low as 2.4 K to above 10 K (Fig. 4, dashed colour lines). Note that the values of β_L and γ_L for the CMIP5 models analysed by Arora et al. (2013) may be scenario or time dependent. Therefore, the variation in G_L with ECS calculated in Figure 4 should be considered illustrative, for the CMIP5 values of β_L and γ_L, and not precise predictions of what would occur in the terrestrial components of the CMIP5 models if run to steady state with CO_2 levels of 410 ppm.

6. Discussion

Two of the most significant sources of uncertainty in the sensitivity of warming to anthropogenic carbon emission arise from uncertainties in the strength of feedbacks operating in the physical climate system (e.g. IPCC, 2013; Knutti et al., 2017) and the land carbon system (e.g. Friedlingstein et al, 2006; Arora et al., 2013). This study shows how, when the land carbon system reaches a new steady state following carbon emission, the strength of these physical climate and terrestrial carbon feedbacks are linked via theoretical relationships (eq. 9, 12) and in numerical model simulations (Figs. 1, 3).

This identified link between terrestrial carbon and physical climate feedbacks implies that the impact on surface warming of the two systems should not be considered in isolation. Firstly, when calculating surface warming from carbon emissions for a different climate feedback one must also consider the impact on terrestrial carbon feedback. For example, an increase in the expected surface warming due to stronger than expected cloud feedback would be compounded by the subsequent reduction in the damping of surface warming from terrestrial carbon feedback (eqns. 9, 10, 12, 14; Fig. 1). Secondly, a significant component of the uncertainty terrestrial carbon feedback arises from the uncertainty in physical climate feedback. In a large observation-constrained ensemble of many thousands of simulations containing significant variation in the carbon cycle responses to rising CO_2 and temperature (Goodwin, 2018; Goodwin et al., 2018), around half the uncertainty in steady state terrestrial carbon feedback (in $Wm^{-2}K^{-1}$) originates from uncertainty in physical climate feedback (Fig. 1b, blue: R^2=0.49).

In the present transient state, the terrestrial carbon feedback appears to be robustly negative with the terrestrial carbon cycle absorbing anthropogenic CO_2 from the atmosphere (le Quéré et al. 2018), and thus reducing anthropogenic warming from carbon emissions. However, the present transient state is also characterized by a lag between rising atmospheric CO_2 and rising surface temperatures, because the transient climate response is lower than the equilibrium climate sensitivity (Knutti et al., 2017; IPCC, 2013). As the terrestrial carbon cycle likely has opposing sensitivities to rising CO_2 and rising temperature (Friedlingstein et al., 2006; Gregory et al., 2009), the future response of the terrestrial carbon uptake depends crucially on the climate sensitivity determining the relative increases in CO_2 and temperature following carbon emission (eqns. 9, 12).

The analysis presented here implies that we may not simply assume that the terrestrial carbon feedback will remain robustly negative at steady state, in line with previous studies finding that the current land carbon sink may become a carbon source over the 21st century or beyond (e.g. Cox et al., 2000; Friedlingstein et al., 2006). There is an increased likelihood that terrestrial carbon feedback will turn positive, enhancing future anthropogenic warming (eq. 12), either at high climate sensitivity (Fig.

1, eqns. 9, 14) or for large warming perturbations caused by increased anthropogenic emissions (Fig. 3, eqns. 12,13).

Appendix A: Model simulations and analysis of model output

This Appendix provides details of how the efficient model simulations are performed, and how the both DVGM and efficient model output is analyzed.

To generate the WASP simulations, the observational constraints of Goodwin (2018) are applied, updated here with a consistency test for land carbon uptake based on the Global Carbon Budget (le Quéré et al. 2018). All consistency tests and ranges remain as in Goodwin (2018), and based on observational constraints on surface warming, ocean heat content, and carbon fluxes (see Goodwin, 2018 - table 2 therein for details), except for the test in in cumulative terrestrial carbon uptake from 1750. The test in cumulative terrestrial carbon uptake since 1750 is applied here in year 2017, and is updated such that the observation-consistent range represents the multi-model mean ± 2 standard deviations in ΔI_{ter} as calculated for 16 observation-consistent Dynamic Global Vegetation Models from the Global Carbon Budget. The best estimate of cumulative carbon uptake ΔI_{ter} over time is calculated using the multi-model mean annual carbon sink values provided in le Quéré et al. (2018). ΔI_{ter} is then calculated separately for each of the 16 Dynamic Global Vegetation Models used in the Global Carbon Budget from le Quéré et al. (2018), using each model's separate annual land carbon sink values (data prior to year 1959 supplied by Stephen Sitch, see Acknowledgements).

The cumulative residual land carbon uptake (excluding carbon emitted from land use change) from preindustrial to 2017 is considered observation consistent if the simulation lies between 96 and 331 PgC, replacing the equivalent terrestrial carbon uptake range in Goodwin (2018 – table 2 therein). All other ranges for observational constraints are as in Goodwin (2018).

When converting simulated terrestrial carbon uptake, ΔI_{ter}, into terrestrial carbon feedback, λ_{carbon}, using eq. (9) the values of a and I_B must be known (Figs 1, 3). To analyse the DGVM simulations of Pugh et al. (2018) values of a=5.35 Wm^{-2} and I_B=3451 PgC are used and $\lambda_{climate}$ is diagnosed using $\lambda_{climate} = a\Delta \ln \mathrm{CO}_2/\Delta T$. For the efficient WASP model simulations the values of a and I_B are considered individually for each ensemble member. The values of $\lambda_{climate}$ evolve over time in the efficient model (Goodwin, 2018), so the values at the end of the 500 year simulations are used (Figs. 1b, 3).

Appendix B: Steady state carbon uptake in the idealized terrestrial carbon system

This Appendix provides the derivation of cumulative terrestrial carbon uptake, ΔI_{ter}, following carbon emission including non-linear interaction between the land carbon responses to rising CO_2 and surface warming, ΔT.

Consider an idealized system consisting of an atmosphere containing CO_2 coupled to a vegetation carbon reservoir and a soil carbon reservoir (Figure 2). The flux of carbon from the atmosphere to the vegetation pool is due to Net Primary Productivity (NPP), F_{NPP} in PgC yr^{-1}. The flux of carbon from the vegetation to the soil carbon pool due to leaf litter, $F_{LeafLitter}$ in PgC yr^{-1}, is equal to the vegetation carbon inventory, I_{veg} in PgC, divided by the vegetation carbon residence timescale, τ_{veg} in yr,

$$F_{LeafLitter} = I_{veg}/\tau_{veg} . \quad \text{(B1)}$$

The flux of carbon from the soil to the atmosphere due to respiration, $F_{Respiration}$, in PgC yr^{-1}, is similarly equal to the soil carbon inventory, I_{soil} in PgC, divided by the soil carbon residence timescale, τ_{soil} in yr,

$$F_{respiration} = I_{soil}/\tau_{soil} . \quad \text{(B2)}$$

These three fluxes must be equal both at the initial steady state, $F_{NPP,0} = F_{Leaflitter,0} = F_{respiration,0}$ (where subscript 0 is used to denote the initial conditions) and once the system reaches a new steady state after perturbation.

At steady state the terrestrial carbon storage, I_{ter} in PgC, is given by the sum of the vegetation and soil carbon reservoirs, also written in terms of the residence timescales using (B1) and (B2),

$$I_{ter} = I_{veg} + I_{soil} = F_{NPP}(\tau_{veg} + \tau_{soil}), \quad \text{(B3)}$$

such that the initial steady state is written $I_{ter,0} = I_{veg,0} + I_{soil,0} = F_{NPP,0}(\tau_{veg,0} + \tau_{soil,0})$.

Next, we assume that F_{NPP} varies from the initial steady state with both the log change in atmospheric CO_2, due to CO_2 fertilization (e.g. Alexandrov et al., 2003), and the global mean surface temperature (e.g. *Friedlingstein et al*., 2006) via,

$$F_{NPP} = F_{NPP,0}(1 + \beta_{CO2}\delta \ln CO_2)(1 + c_{NPP}\delta T), \quad \text{(B4)}$$

where β_{CO2} is the empirically determined dimensionless CO_2 fertilization coefficient relating the sensitivity of NPP to the log change in CO_2 (Alexamdrov et al., 2003); and c_{NPP} is the empirically determined fractional sensitivity of NPP to global mean surface temperature in K^{-1}.

Soil carbon residence time is also known to be sensitive to global mean surface temperature due to temperature effects on microbial respiration (e.g. *Friedlingstein et al.*, 2006). Here, we assume an idealized relationship,

$$\tau_{soil} = \tau_{soil,0}(1 + c_{soil}\delta T), \quad \text{(B5)}$$

where c_{soil} is the empirically determined fractional sensitivity of soil carbon residence time to global mean surface temperature in K^{-1}.

Substituting (B4) and (B5) into (B3) reveals the final steady state terrestrial carbon reservoir, $I_{ter} = I_{ter,0} + \delta I_{ter}$, following a perturbation to atmospheric CO_2 and temperature,

$$I_{ter,0} + \Delta I_{ter} = F_{NPP,0}(1 + \beta_{CO2}\delta \ln \mathrm{CO_2})(1 + c_{NPP}\delta T)\big(\tau_{veg,0} + \tau_{soil,0}[1 + c_{soil}\delta T]\big). \quad \text{(B6)}$$

For the idealized CO_2-only forcing scenario considered here, the values of δT and $\delta \ln CO_2$ at steady state are related via the CO_2 radiative forcing coefficient, a (Myhre et al., 2013), and the physical climate feedback $\lambda_{\mathrm{climate}}$, eq. (3). Substituting $\delta T = a\delta \ln \mathrm{CO_2}/\lambda_{climate}$ into (B6) reveals an expression for the final steady state terrestrial carbon storage in in terms of the perturbation to δT following carbon emission,

$$I_{ter} = F_{NPP,0}\left(1 + \frac{\lambda_{climate}}{a}\beta_{CO2}\delta T\right)(1 + c_{NPP}\delta T)\big(\tau_{veg,0} + \tau_{soil,0}[1 + c_{soil}\delta T]\big). \quad \text{(B7)}$$

Subtracting the initial terrestrial carbon storage, $I_{ter,0} = F_{NPP,0}(\tau_{veg,0} + \tau_{soil,0})$, from (B7) solves for the change in terrestrial carbon storage since preindustrial, δI_{ter}, revealing a third order polynomial in δT,

$$\delta I_{ter} = F_{NPP,0}\left[\left\{\tau_{veg,0}\left(\frac{\lambda_{climate}}{a}\beta_{CO2} + c_{NPP}\right) + \tau_{soil,0}\left(\frac{\lambda_{climate}}{a}\beta_{CO2} + c_{NPP} + c_{soil}\right)\right\}\delta T + \left\{\tau_{veg,0}\frac{\lambda_{climate}}{a}\beta_{CO2}c_{NPP} + \tau_{soil,0}\left(\frac{\lambda_{climate}}{a}\beta_{CO2}[c_{NPP} + c_{soil}] + c_{NPP}c_{soil}\right)\right\}\delta T^2 + \left\{\tau_{soil,0}\frac{\lambda_{climate}}{a}\beta_{CO2}c_{NPP}c_{soil}\right\}\delta T^3\right] \quad \text{(B8)}$$

Equations (B1), (B2) and (B8) are then substituted into eq. (9), $\lambda_{carbon} = -\frac{\delta R_{CO2}^{ter}}{\delta T} = \frac{a}{I_B}\frac{\delta I_{ter}}{\delta T}$, to solve for λ_{carbon}, revealing eq. (12).

Acknowledgements and Data: This work was supported by UK NERC grant NE/N009789/1. The author declares no competing financial interests. Thanks are given to Stephen Sitch for supplying the simulated annual carbon sink values for the 16 individual DVGMs used in the Global Carbon Project analysis for years prior to 1959. This was used to construct the updated observational constraint for cumulative land carbon uptake applied the WASP simulations. The computer code for the version of the WASP Earth system model used in this study, able to replicate all new experiments performed here, is publicly available within Goodwin (2018 – supporting information therein).

References:

Alexandrov, G., Oikawa, T., and Yagamata, Y. (2003) Climate dependence of the CO_2 fertilization effect on terrestrial net primary production, *Tellus B*, 55, 669-675.

Archer, D. (2005), The fate of fossil fuel in geologic time, *J. Geophys. Res*., 110, C09S05, doi:10.1029/2004JC002625.

Arora, V.K., Boer, G.J., Friedlingstein, P., Eby, M., Jones, C.D., Christian, J.R., Bonan, G., Bopp, L., Brovkin, V., Cadule, P. and Hajima, T. (2013) Carbon–concentration and carbon–climate feedbacks in CMIP5 Earth system models. *J. Climate*, 26(15), pp.5289-5314.

Balmaseda, M. A., Mogensen, K., & Weaver, A. T. (2013). Evaluation of the ECMWF ocean reanalysis system ORAS4. *Quarterly Journal of the Royal Meteorological Society*, 139, 1132–1161.

Cheng, L., Trenberth, K. E., Fasullo, J., Boyer, T., Abraham, J., & Zhu, J. (2017). Improved estimates of ocean heat content from 1960 to 2015. *Science Advances*, 3, e1601545.

Cox, P., Betts, R.A., Jones, C.D., Spall, S.A. and Totterdell, I.J. (2000). Acceleration of global warming due to carbon-cycle feedbacks in a coupled climate model, *Nature* 408, 184-187.

Friedlingstein, P., Cox, P., Betts, R., Bopp, L., von Bloh, W., Brovkin, V., … and Bala, G., (2006) Climate–carbon cycle feedback analysis: results from the C4MIP model intercomparison. *J. Climate*, *19*(14), pp.3337-3353.

Giese, B. S., & Ray, S. (2011). El Niño variability in simple ocean data assimilation (SODA), 1871–2008. *Journal of Geophysical Research*, 116, C02024. https://doi.org/10.1029/2010JC006695

Good, S. A., Martin, M. J., & Rayner, N. A. (2013). EN4: quality controlled ocean temperature and salinity profiles and monthly objective analyses with uncertainty estimates. *Journal of Geophysical Research: Oceans*, 118, 6704–6716. https://doi.org/10.1002/2013JC009067

Goodwin, P., (2018) On the time evolution of climate sensitivity and future warming, *Earth's Future* 6, 1336-1348, doi:10.1029/2018EF000889.

Goodwin, P., Williams, R. G., Roussenov, V. M., & Katavouta, A. (2019). Climate sensitivity from both
physical and carbon cycle feedbacks. *Geophysical Research Letters*, 46.
https://doi.org/10.1029/2019GL082887

Goodwin, P., Katavouta, A., Roussenov, V.M., Foster, G.L., Rohling, E.J., and Williams, R.G. (2018) Pathways to 1.5 and 2 °C warming based on observational and geological constraints, *Nature Geoscience* 11, 102-107, doi:10.1038/s41561-017-0054-8.

Goodwin, P. (2016) How historic simulation-observation discrepancy affects future warming projections in a very large model ensemble, *Climate Dynamics*, CLDY-D-15-00368R2, doi: 10.1007/s00382-015-2960-z.

Goodwin, P., Williams, R.G., and Ridgwell, A. (2015), Sensitivity of climate to cumulative carbon emissions due to compensation of ocean heat and carbon uptake, *Nature Geoscience* 8, 29-34. doi:10.1038/ngeo2304.

Goodwin, P., and Ridgwell, A. (2010), Ocean-atmosphere partitioning of anthropogenic carbon dioxide on multimillennial timescales, *Global Biogeochem. Cycles*, 24, GB2014, doi:10.1029/2008GB003449.

Goodwin, P., Williams, R.G., Ridgwell, A., and Follows, M.J. (2009), Climate sensitivity to the carbon cycle modulated by past and future changes in ocean chemistry, *Nature Geoscience*, Vol. 2, No. 2, p145-150, doi:10.1038/ngeo416.

Goodwin, P., M. J. Follows, R. G. Williams (2008), Analytical relationships between atmospheric carbon dioxide, carbon emissions, and ocean processes, *Global Biogeochemical Cycles*, 22, GB3030, doi:10.1029/2008GB003184.

Goodwin, P., R.G. Williams, M.J. Follows, S. Dutkiewicz (2007), Ocean-atmosphere partitioning of anthropogenic carbon dioxide on centennial timescales, *Global Biogeochemical Cycles*, 21, GB1014, doi:10.1029/2006GB002810.

Gregory, J. M., Jones, C. D., Cadule, P. & Friedlingstein, P. (2009) Quantifying carbon cycle feedbacks. *J. Clim*. 22, 5232–5250.

Hansen, J., Ruedy, S., Sato, M., & Lo, K. (2012). Global surface temperature change. *Reviews of Geophysics*, 48, RG4004. https://doi.org/10.1029/2010RG000345

IPCC (2013) *Climate Change 2013: The Physical Science Basis* (eds Stocker, T. F. et al.) Cambridge Univ. Press, Cambridge, UK.

Knutti, R., Rugenstein, M.A.A. and Hergerl, G.C. (2017) Beyond equilibrium climate sensitivity, *Nature Geoscience* 10, 727-736, DOI:10.1038/ngeo3017.

le Quéré et al. (2018). Global Carbon Budget 2017, *Earth Syst. Sci. Data*, 10, 405-448, https://doi.org/10.5194/essd-10-405-2018.

Levitus, S., Antonov, J. I., Boyer, T. P., Baranova, O. K., Garcia, H. E., Locarnini, R. A., et al. (2012). World ocean heat content and thermosteric sea level change (0–2000 m), 1955–2010. *Geophysical Research Letters*, 39, L10603. https://doi.org/10.1029/2012GL051106

MacDougall, A.H. and Knutti, R. (2016) Projecting the release of carbon from permafrost soils using a perturbed physics ensemble modelling approach. *Biogeosciences*, 13, 2123–2136, doi:10.5194/bg-13-2123-2016.

Morice, C. P., Kennedy, J. J., Rayner, N. A., & Jones, P. D. (2012). Quantifying uncertainties in global and regional temperature change using an ensemble of observational estimates: the HadCRUT4 dataset. *Journal of Geophysical Research*, 117, D08101. https://doi.org/10.1029/2011JD017187

Myhre, G., D. Shindell, D., Bréon, F.-M., Collins, W. J., Fuglestvedt, J.,Huang, J. et al. (2013) Anthropogenic and Natural Radiative Forcing. In: *Climate Change 2013: The Physical Science Basis. Contribution of Working Group I to the Fifth Assessment Report of the Intergovernmental Panel on Climate Change* [Stocker, T.F., D. Qin, G.-K. Plattner, M. Tignor, S.K. Allen, J. Boschung, A. Nauels, Y. Xia, V. Bex and P.M. Midgley (eds.)].

Nichols, R.J., Brown, S., Goodwin, P., Wahl, T., Lowe, J., Solan, M. et al. (2018) Stabilization of global temperature at 1.5°C and 2°C: implications for coastal areas, *Phil. Trans. R. Soc. A*, 376, 20160448.
http://dx.doi.org/10.1098/rsta.2016.0448.

Pugh, T. A. M., Jones, C. D., Huntingford, C., Burton, C., Arneth, A., Brovkin, V., et al. (2018). A large committed long-term sink of carbon due to vegetation dynamics. *Earth's Future,* 6. https://doi.org/10.1029/2018EF000935.

Schuur, E., McGuire, A.D., Schädel, C., Grosse, G., Harden, J.W., Hayes, D.J., et al., (2015) Climate change and the permafrost carbon feedback. *Nature,* 520 (7546), 171–179. doi:10.1038/nature14338.

Smith, D. M., Allan, R. P., Coward, A. C., Eade, R., Hyder, P., Liu, C., et al. (2015). Earth's energy imbalance since 1960 in observations and CMIP5 models. *Geophysical Research Letters*, 42, 1205–1213. https://doi.org/10.1002/2014GL062669.

Smith, T. M., Reynolds, R. W., Peterson, T. C., & Lawrimore, J. (2008). Improvements to NOAA's historical merged land–ocean surface temperature analysis (1880–2006). *Journal of Climate*, 21, 2283–2296.

Vose, R. S., Arndt, D., Banzon, V. F., Easterling, D. R., Gleason, B., Huang, B., et al. (2012). NOAA's merged land–ocean surface temperature analysis. *Bulletin of the American Meteorological Society*, 93, 1677–1685.

Williams, R. G., P. Goodwin, A. Ridgwell, and P. L. Woodworth (2012), How warming and steric sea level rise relate to cumulative carbon emissions, *Geophys. Res. Lett.*, 39, L19715, doi:10.1029/2012GL052771.

Williams, R.G., Roussenov, V., Goodwin, P., Resplandy, L. and Bopp, L. (2017) Sensitivity of global warming to carbon emissions: effects of heat and carbon uptake in a suite of Earth system models, *Journal of Climate* 30, 9343-9363, doi:10.1175/JCLI-D-16-0468.1

Zeebe, R.E. and Wolf-Gladrow, D. (2001) *CO_2 in Seawater: Equilibrium, Kinetics, Isotopes*, Elsevier Oceanography Series Vol. 65, Amsterdam, The Netherlands.

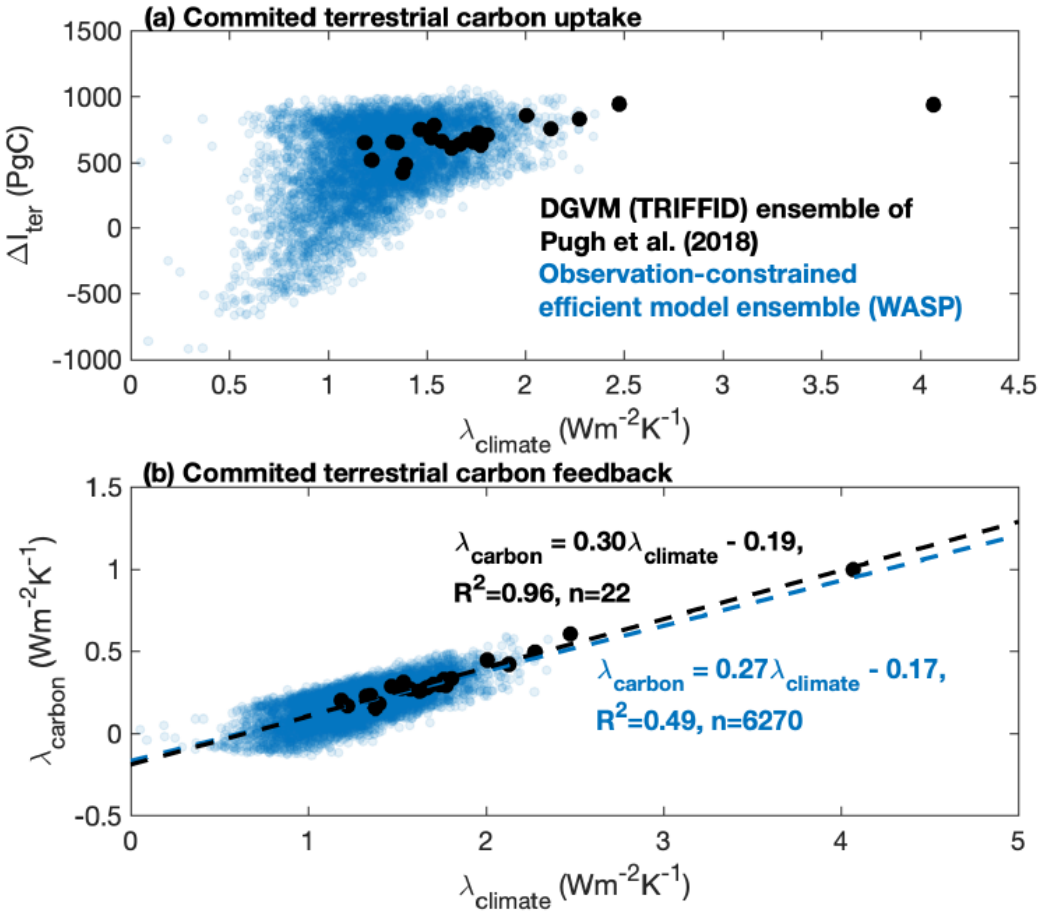

906

Figure 1: Terrestrial carbon uptake and feedback varies with physical climate feedback at fixed ΔCO_2 perturbation. (a) Cumulative terrestrial carbon uptake at steady state, ΔI_{ter}, following fixed ΔCO_2 perturbations at different climate feedback, $\lambda_{climate}$, in a complex DGVM (black) and an efficient model ensemble (blue). (b) The terrestrial carbon feedback, λ_{carbon}, at different physical climate feedback, $\lambda_{climate}$, for the model simulations (dots) showing an emergent relationship between terrestrial carbon feedback and physical climate feedback in two model ensembles (dashed lines).

908

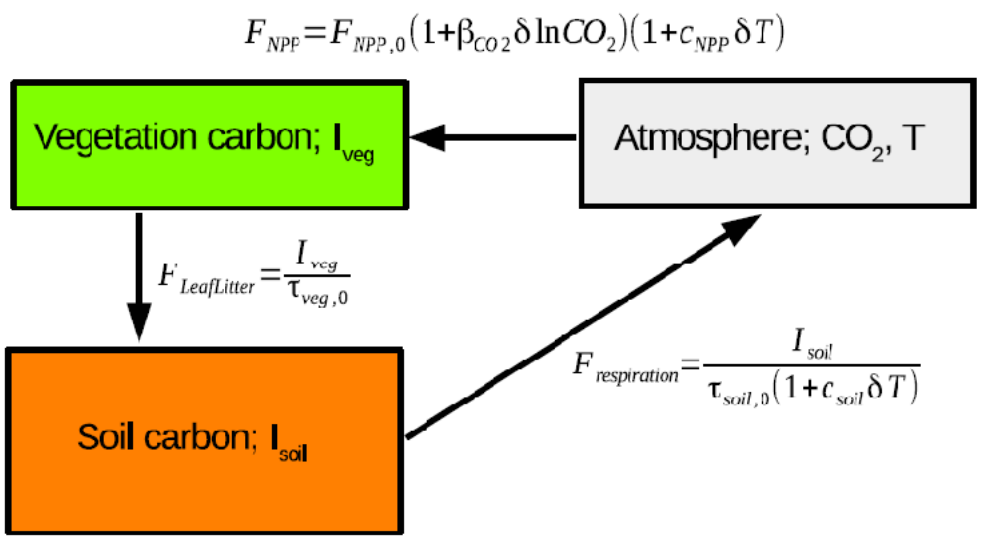

910

Figure 2: Schematic of an idealised two-box representation of the terrestrial carbon cycle. Vegetaion and soil carbon reservoirs are attached to an atmosphere with atmospheric CO_2 and global mean surface temperature T. F_{NPP} is the Net Primary Productivity carbon flux in PgC yr^{-1}, $F_{leaflitter}$ is the leaf litter carbon flux in PgC yr^{-1} and $F_{respiration}$ is the soil carbon respiration flux in PgC yr^{-1}. I_{veg} and I_{soil} are the vegetation and soil carbon inventories respectively in PgC, while $\tau_{soil,0}$ and $\tau_{veg,0}$ are the initial vegetation and soil carbon residence timescales respectively in yrs. Carbon fluxes are sensitive to atmospheric CO_2, via β_{CO2}, and temperature, via c_{NPP} in K^{-1} and c_{soil} in K^{-1}.

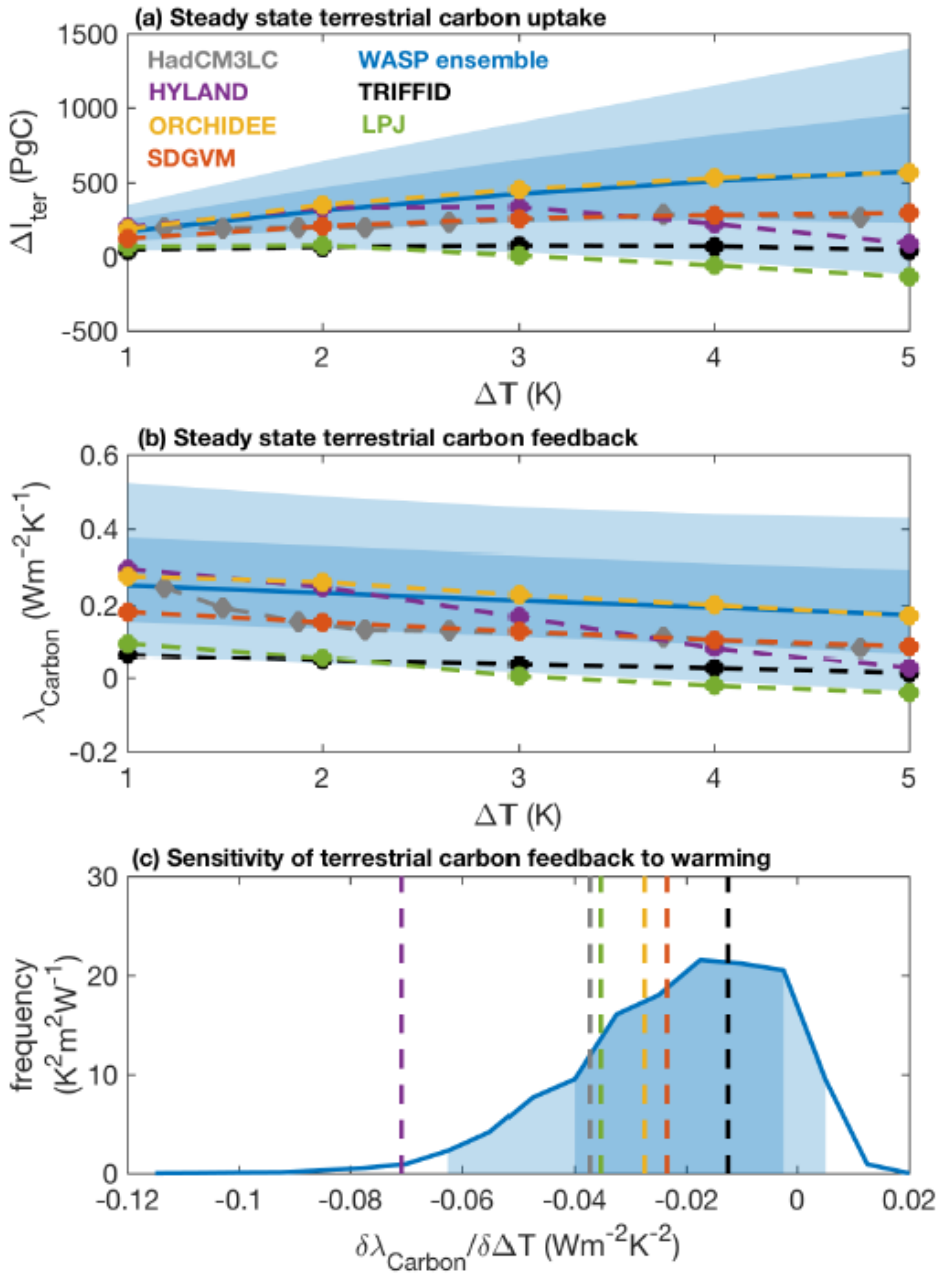

912

Figure 3: Terrestrial carbon uptake and terrestrial carbon feedback varies with surface warming at fixed physical climate feedback. (a) Cumulative terrestrial carbon uptake at steady state, ΔI_{ter}, following different carbon emission sizes leading to different surface warming, ΔT. (b) The steady state terrestrial carbon feedback, λ_{carbon} in $Wm^{-2}K^{-1}$, for different carbon emission sized leading to different surface warming, ΔT. (c) The sensitivity of λ_{carbon} to surface warming in a large ensemble of efficient model simulations (frequency density plot: blue solid line and shading), and in individual models (dashed lines). Sensitivities in (c) represent the gradient of the line of best fit for each model in panel (b).

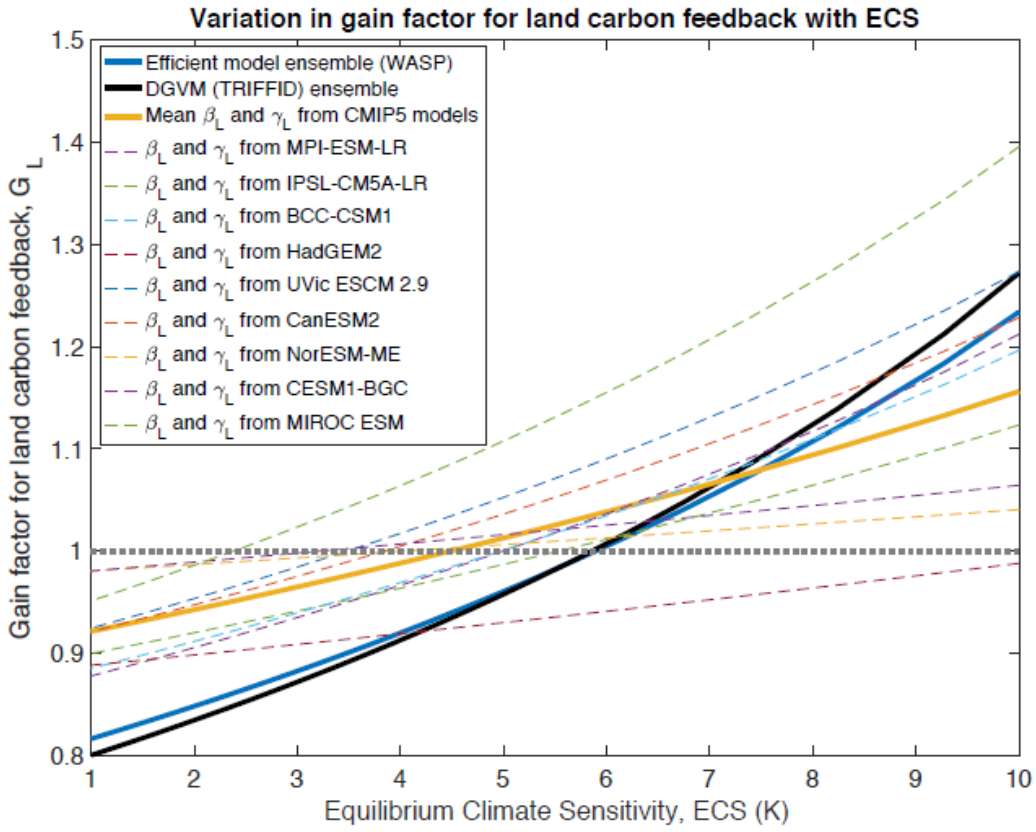

916

Figure 4: Steady state gain in surface warming due to land carbon feedback varies with Equilibrium Climate Sensitivity for a given CO_2 stabilisation. The gain G_L as a function of Equilibrium Climate Sensitivity (ECS) is calculated from equation (14) for different relationships between $\lambda_{climate}$ and λ_{carbon}, and for different β_L and γ_L values. For the efficient WASP model ensemble (solid blue line) and the DGVM TRIFFID model ensemble of Pugh et al. (2018) (solid black line), G_L is calculated as a function of ECS using the relationships between $\lambda_{climate}$ and λ_{carbon} identified in fig. 1b (eq. 14). G_L is calculated as a function of ECS using values of β_L and γ_L identified by Arora et al. (2013) for the CMIP5 ensemble mean (solid orange line) and individual CMIP5 models (dashed colour lines). Equation (14) is then applied assuming climate is stabilised with approximately present-day CO_2 levels of 410 ppm in (eq. 14).